Light Metals 2014
Edited by: John Grandfield
TMS (The Minerals, Metals & Materials Society), 2014

Modelling of Micro- and Macrosegregation in Multicomponent Aluminium Alloys Accounting for Secondary Phase Formation

K.Ellingsen[1], Mohammed M'Hamdi[1], Knut Tveito[2] and Dag Mortensen[3]
[1]SINTEF Materials and Chemistry, Oslo, N-0314, Norway
[2]Norwegian University of Science and Technology, Trondheim, N-7034, Norway
[3]Institute for Energy Technology, Kjeller, N-2027, Norway

Keywords: DC-casting, macrosegregation, modeling, multicomponent alloys

Abstract

Realistic predictions of macrosegregation formation during solidification of aluminium alloys require an accurate modeling of solute microsegregation accounting for multicomponent phase diagrams and secondary phase formation. In the present work, the stand alone ALSTRUC model, a microsegregation model for industrial multicomponent aluminium alloys, is coupled with the continuum model ALSIM which calculates the macroscopic transport of mass, enthalpy, momentum, and solutes during solidification of aluminium. Alstruc deals with multicomponent alloys accounting for temperature dependent partition coefficients, liquidus slopes and the precipitation of secondary phases. The challenge associated with computation of microsegregation for multicomponent alloys is solved in ALSTRUC by approximating the phase diagram data by simple, analytical expressions which allows for a CPU-time efficient coupling with the macroscopic transport model. In the present work, a coupling strategy is proposed where macroscopic transport quantities such as the enthalpy and the solute compositions are used as input to the microsegregation model which then returns the temperature, solid fraction and the compositions in the solid and the liquid phases. The coupled solidification model is then applied in a case study to illustrate the effect of secondary phase precipitation on macrosegregation formation due to shrinkage induced flow.

Introduction

Macrosegregation, the non-homogeneous chemical composition on the length scale of the casting, is one of several possible defects in casting. Mathematical models quantifying the formation of macrosegregation are well-established and based on mixing theory or volume-averaging of the conservation laws for mass, solute mass, enthalpy, and momentum [3]. These models need a sub-model by which the values of the liquid fraction and solute concentrations or their variations in the liquid phase in a given volume element are related to the values of the enthalpy (or temperature) and total solute concentrations. The basis for these solidification path models is a microsegregation model that calculates the solute concentration in the dendrite (arm) during the solidification process as well as the amount and composition of the secondary phases that precipitate. Microsegregation models need input from thermodynamical phase diagrams. Although databases for multicomponent aluminium alloys [4-7] are available, m*ulti-component* microsegregation models have only to a limited extent been coupled to macrosegregation models [8-12]. Macrosegregation development implies a change in the total solute concentration in the volume elements and it is not possible to use a unique solidification path throughout the whole casting. The solidification path needs to be updated at each time step and for each volume element of the macro model. This can be quite computer time and storage demanding as the microsegregation model also needs updated phase diagram data.

In the present work, the ALSTRUC model, a microsegregation model for industrial multicomponent aluminium alloys, is extended for application as a micro-module for macrosegregation computations. The module is coupled with the continuum model ALSIM which calculates the macroscopic transport of mass, enthalpy, momentum, and solute in aluminium casting. The challenge associated with computation of microsegregation for multicomponent alloys is solved in ALSTRUC by approximating the phase diagram data by simple, analytical expressions which allows for a CPU-time efficient coupling with the macroscopic transport model. Preliminary assessments demonstrating the usefulness of the new module has been presented elsewhere [15, 26]. In this study the coupled models are applied in a simplified DC-casting study.

Model description

ALSIM

Alsim [2,16,17] calculates the development of heat, fluid flow, stresses, and deformation during casting. For aluminium DC casting situations, the model addresses the thermal and fluid flow boundary conditions to a very high level of details regarding contact zones, air gap sizes, and water hit points. This also includes the effect upon the surface heat transfer and associated surface exudation caused by air-gap formation [17, 18]. Alsim also address the formation of macrosegregation. For a fixed solid ($\mathbf{v}_s=\mathbf{0}$) the mass and momentum equations are given by:

$$\frac{\partial}{\partial t}\rho + \nabla\cdot\left(\rho^l g^l \mathbf{v}^l\right) = 0 \tag{1}$$

$$\begin{aligned}&\frac{\partial}{\partial t}\left(g^l\mathbf{v}^l\right) + \nabla\cdot\left(g^l\mathbf{v}^l\mathbf{v}^l\right) = -\frac{g^l}{\rho^l}\nabla p^l \\ &+\nabla\left[\nu\left(\nabla\left(g^l\mathbf{v}^l\right)+\left[\nabla\left(g^l\mathbf{v}^l\right)\right]^t\right)\right] + \frac{g^l}{\rho^l}\mathbf{g}(\Delta\rho^l) - \frac{g^l\nu}{K}\left(g^l\mathbf{v}^l\right)\end{aligned} \tag{2}$$

where ρ, ρ^l, ρ^s, g^l, g^s, v^l, p^l, ν, f_i^l , g and K are the mixture density ($\rho = \rho^l g^l + \rho^s g^s$), liquid density (assumed constant except in the buoyancy term using the Boussinesq approximation), solid density, liquid volume fraction, solid volume fraction, liquid velocity, liquid pressure, kinematic viscosity, gravity vector and permeability, respectively. Solidification shrinkage, interfacial friction, and macroscopic viscous stress contribution are included. For the sake of simplicity, the contribution from thermo-solutal

convection is neglected here. For solute conservation the following mixture equations are applied:

$$\frac{\partial}{\partial t}(\rho \cdot c_i) + \nabla \cdot \left(\rho^l g^l c_i^l \mathbf{v}^l\right) = \nabla \cdot (\rho D_i \nabla c_i) \quad (3)$$

where c_i is the mixture concentration for element i, and $\rho c^i = \rho^l g^l c_i^l + \rho^s g^s c_i^s$. D_i is the mixture diffusion constant and $\rho D_i = \rho^l g^l D_i^l + \rho^s g^s D_i^s$. The term in the right-hand side of Eq. (3) is added for numerical stability reasons. Similar for energy conservation the following mixture enthalpy equation is applied:

$$\frac{\partial}{\partial t}(\rho \cdot h) + \nabla \cdot \left(\rho^l g^l h^l \mathbf{v}^l\right) = \nabla \cdot (\lambda \nabla T) \quad (4)$$

where h is the mixture enthalpy and $\rho \cdot h = \rho^l g^l h^l + \rho^s g^s h^s$, and λ is the mixture thermal conductivity ($\lambda = g^l \lambda^l + g^s \lambda^s$).

ALSTRUC

ALSTRUC [1] calculates the solidification path of AlMgCuFeMnSi alloys in the Al rich corner of the phase diagram. ALSTRUC also handles additions of Cr, V, Sr, Ti, and Zn in commercial alloys. The model uses the well-established assumptions of full miscibility in the liquid and thermodynamic equilibrium at the solid/liquid interface and accounts for solid-state diffusion and particle growth undercooling. A constant total alloy composition is input along with the cooling rate and the final characteristic dendrite arm length. By gradually changing the solid fraction in a step-wise manner, Alstruc computes the solute concentrations in the liquid phase, the temperature, the alloying element concentration profiles and the amount and composition of the various secondary phases in a simplified geometrical representation of the dendrite arm. Phase diagrams are formulated as simple, approximate, analytical expressions. Computer time and storage demanding calls to a thermodynamic data base, or alternatively, use of numerical mapping of such data [9,11], is thus avoided. The amount and concentration of the secondary phases are calculated at the end of each step by considering solubility products assuming that all secondary phases are precipitated from the liquid phase. The model parameters have been tuned to metallographic investigations of solidification microstructures in samples from numerous experiments [20-25].

The ALSTRUC/ALSIM coupling

The ALSIM/ALSTRUC coupling is carried out through a dynamically linked library (DLL). The solid phase diffusion of the alloying elements in the dendrite arms is neglected (Scheil-Gulliver approximation). This simplification also keeps the computation time and data storage low because the alloy concentration profiles do not need to be traced at the nodal points of Alsim. Input to the micro-model are the Alsim predicted values of the enthalpy and average alloy compositions at the start and end of the time step along with values for the solid fraction, alloying element concentrations in the liquid phase, and temperature at the beginning of the step. To compute the change in solid fraction, the Alstruc micro-model requires the change in liquid composition without considering solidification as input. The latter is computed from the total average concentration at the end of the time step in the following manner:

$$c_i^{l\,Alstruc} = (c_i(t) - f^s(t\text{-}1) \cdot c_i^s(t\text{-}1)) / (f^s(t\text{-}1) - 1) \quad (5)$$

where $c_i(t)$ is the average total concentration at the end of the step, $f^s(t\text{-}1)$ *is* the fraction of solid and $c_i^s(t\text{-}1)$ the composition of the solid at the beginning of the step. The approach is justified by the different time and length scales of the macroscopic and microscopic concentration changes.

The solid fraction, alloying element concentrations in the liquid phase and temperature at the end of the time step are calculated by integrating differential versions of the Scheil-Gulliver-like equations before precipitation of secondary phases.

Model application

The model is applied to study the macrosegregation formation in DC cast round billets with ingot diameter 315 mm. The casting speed is kept constant at 50 mm/min. The 2D axisymmetric solution domain is shown in Figure 1. Simplified inlet and heat transfer conditions are applied as defined in Figure 1 where the secondary cooling is given by [27]:

$$h_{Secondary}(T) = \left(-16700 + 352(T - T_{water})\right) \cdot \left(\frac{Q_{water}}{P}\right)^{\frac{1}{3}} + 20.8\left(\frac{(T - T_{saturation})^3}{T - T_{water}}\right) \quad (6)$$

The water flow rate, Q, is 40 l/min. The simulations are transient including heat transfer, shrinkage induced flow and macrosegregation and run until steady state. The steady state macrosegregation patterns will be discussed.

A 5182 alloy (Al-4wt%Mg-0.4wt%Mn-0.2wt%Si-0.3wt%Fe-0.1wt%Cu) is studied. In order to study the effect of secondary phase precipitation on the macrosegregation formation, two different cases are studied: a) the Alstruc module is employed but precipitation of secondary phases is omitted and b) the full Alstruc module is employed. Figure 2 show the development of the compositions of the remaining liquid during solidification at the nominal alloy composition both including (solid lines) and omitting (dashed lines) precipitation of secondary phases. When secondary phases are not accounted for, the liquid concentrations increase during solidification as the solute elements are less soluble in the solid. Accounting for secondary phases, changes the development of the liquid concentration of Mn, Fe, Si and Cu. Precipitation of Mn- and Fe-containing secondary phases starts at a solid fraction of approximately 0.40, and the concentration of Mn and Fe in the remaining liquid therefore decreases from then onwards. Precipitation of Si-containing secondary phases start from a solid fraction of 0.9 and Cu-containing particles from a solid fraction of 0.98.

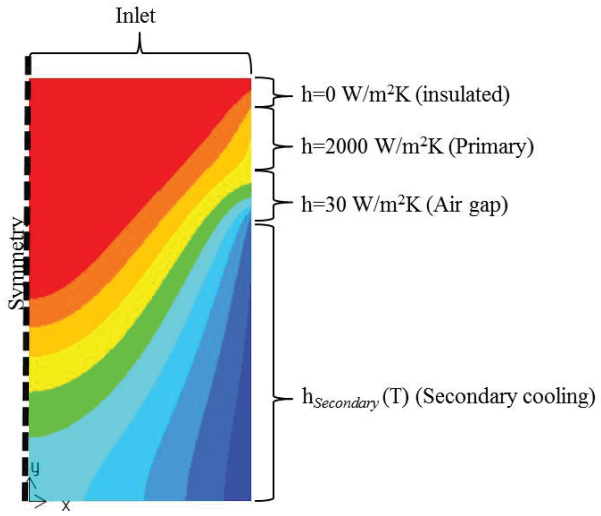

Figure 1: Case definition

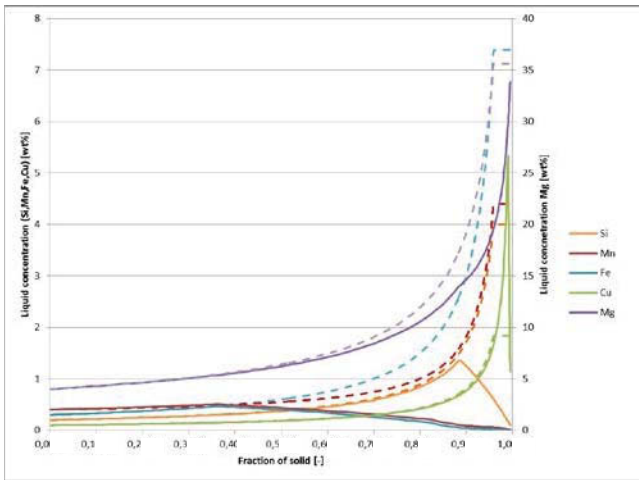

Figure 2: a) Alloy compositions of the liquid phase as a function of the solid fraction during solidification the 5182 at nominal composition (no macrosegregation). Data accounting for secondary phases are shown with solid lines, whereas data where secondary phase precipitation is omitted are shown with dashed lines.

Results

The computed Mg segregation pattern is shown in Figure 3.a, whereas the concentration profile from the center to the surface of the ingot is shown if Figure 3b. The segregation pattern in case a) and b) are similar. Along the surfaces of the ingot a positive segregation is obtained (~10 % for both cases) due to the inverse segregation phenomenon. In the ingot centre, 6 % (case a) and 7 % (case b) negative relative macrosegregation is obtained due to solidification shrinkage.

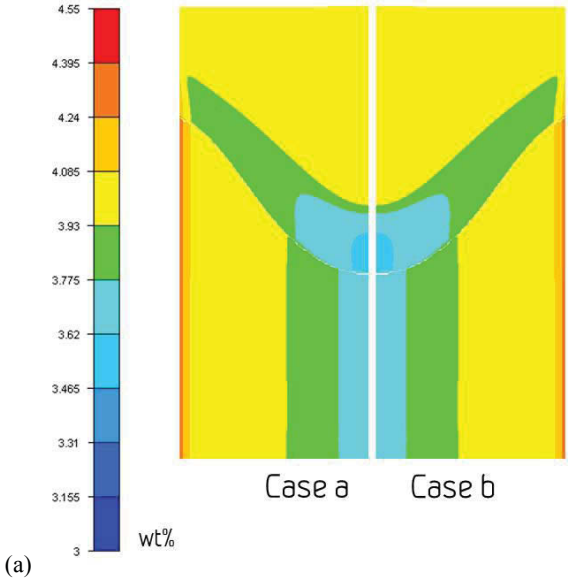

(a)

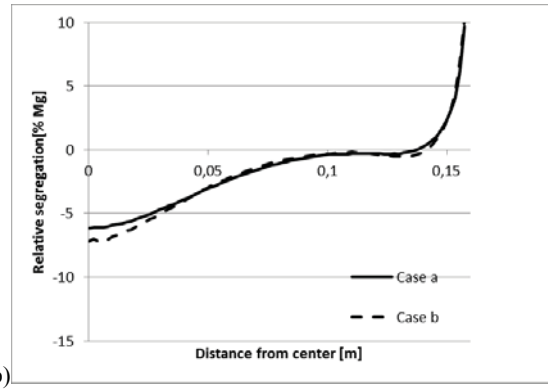

(b)

Figure 3: Mg segregation. a) Segregation pattern (wt %) for case a and b (white line at f_s=1). b) Segregation (%) in the steady state from center to surface of the ingot.

The computed Mn segregation pattern is shown in Figure 4.a, whereas the concentration profile from the center to the surface of the ingot is shown if Figure 4b. Along the surfaces of the ingot ~9% positive segregation is obtained for case a, but a slight negative segregation of ~1 % is calculated for case b. In the center of the ingot, ~5% negative segregation is obtained for case a, however, a slight positive segregation (0.7 %) is obtained for case b. The difference between case a and b can be explained by the precipitation of the Al_6(Mn,Fe) phase. The Al_6(Mn,Fe) precipitation starts at a solid fraction of approximately 0.4 and the concentration of Mn in the remaining liquid decreases from then onwards (Figure 2). Plotting the vertical average Mn concentration in the center of the ingot, from the fully liquid fully solid, (figure 4c), we find that the concentration of Mn decreases with solid fraction until formation of the eutectic, ending up with a negative center for case a). For case b), the average Mn concentration decreases until precipitation of the Al_6(Mn,Fe) phase, and increases before a slight decrease, ending up with a spositive center. Similarly, plotting the average concentration from the fully liquid perpendicular to the isotherms in the surface region of the ingot (figure 4c), we find an increase in the average concentration for case a) as the surface region is fed by liquid

enriched with Mn. For case b), the concentration increases slightly before it decreases as the liquid has lower Mn content due to the precipitation of $Al_6(Mn,Fe)$.

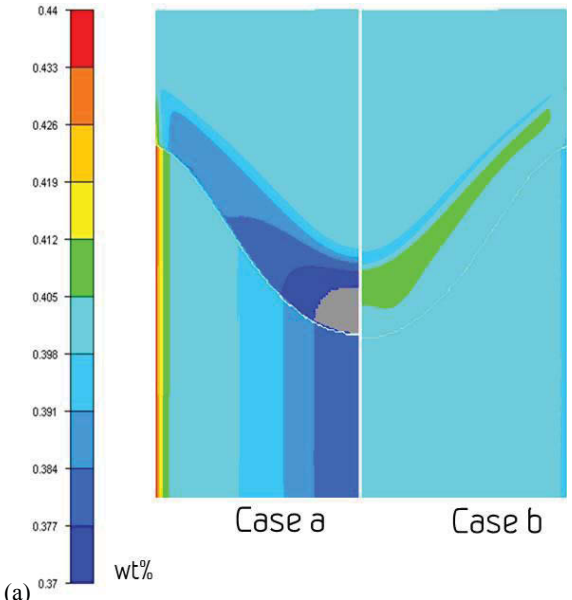

(a)

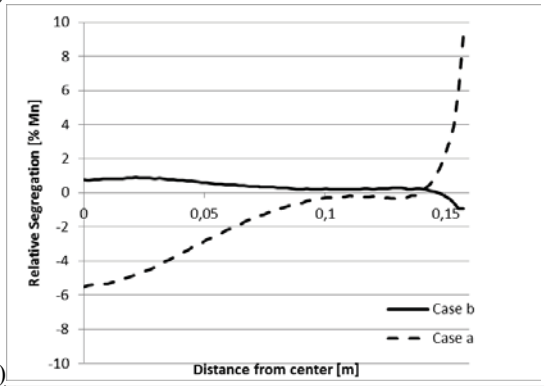

(b)

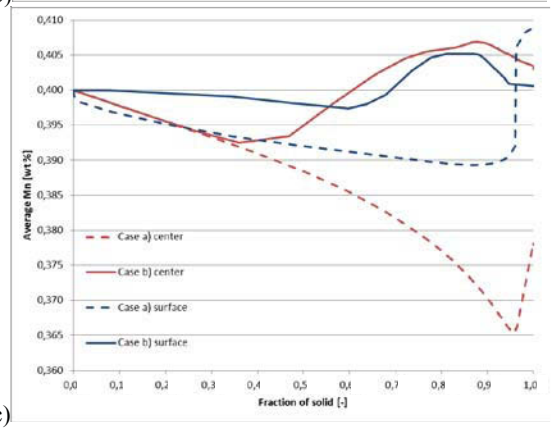

(c)

Figure 4: Mn segregation. a) Segregation pattern (wt %) for case a and b (white line at fs=1). The grey area is out of range (minimum value of 0.365 wt%). b) Segregation (%) in the steady state from center to surface of the ingot c) Average concentration profile from fully liquid to fully solid through ingot center (red lines) and at towards the ingot surface perpendicular to the isotherms (blue lines).

The computed Fe segregation pattern is shown in Figure 5a, whereas the concentration profile from the center to the surface of the ingot is shown if Figure 5b. Along the surfaces of the ingot ~23% positive segregation is obtained for case a) and a slight negative segregation ~0.3 % for case b). In the center of the ingot, ~15% negative segregation is obtained for case a) and a slight negative segregation (0.2 %) is obtained for case b). The difference between case a) and b) can as for Mn be explained by the precipitation of the $Al_6(Mn,Fe)$ phase changing the distribution of Fe between the solid and liquid phase during solidification.

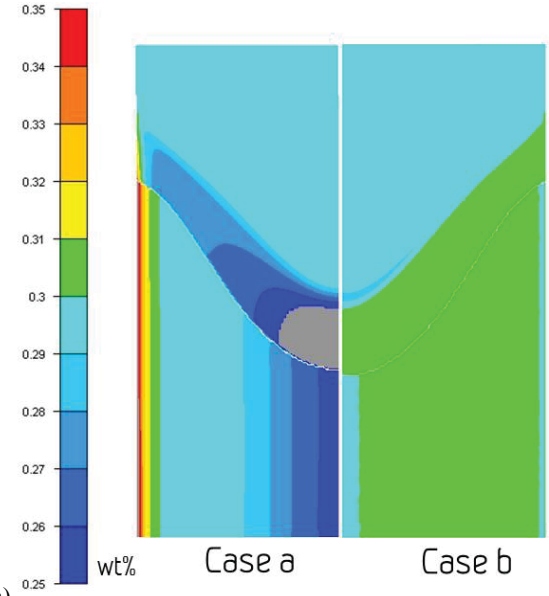

(a)

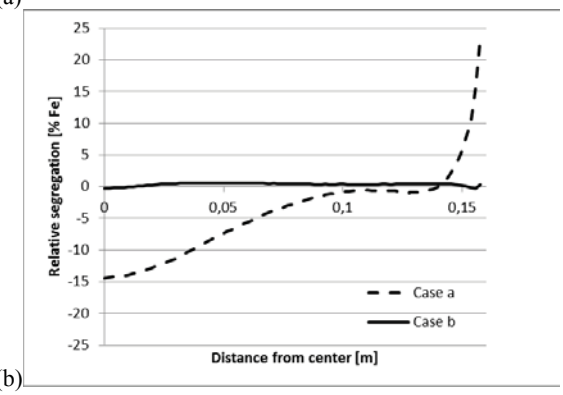

(b)

Figure 5: Fe segregation. a) Segregation pattern (wt %) for case a and b (white line at fs=1). The grey area is out range (minimum value 0.23 wt%). b) Segregation (%) in the steady state from center to surface of the ingot.

The computed Si segregation pattern is shown in Figure 6a, whereas the concentration profile from the center to the surface of the ingot is shown if Figure 6b. Along the surfaces of the ingot ~20% and ~8% positive segregation is obtained for case a) and b) respectively. In the center of the ingot, ~12% and 7% negative segregation is obtained for case a) and b) respectively. The difference between case a) and b) can be explained by the precipitation of the Mg_2Si phase. The precipitation starts at a solid fraction of approximately 0.9 and the concentration of Si in the remaining liquid decreases from then onwards (Figure 2) which

reduces the positive segregation at the surface and the negative segregation in the center for case b).

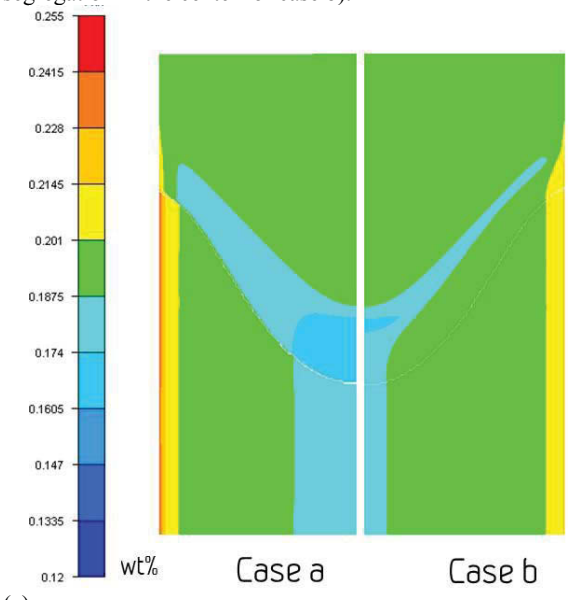

(a)

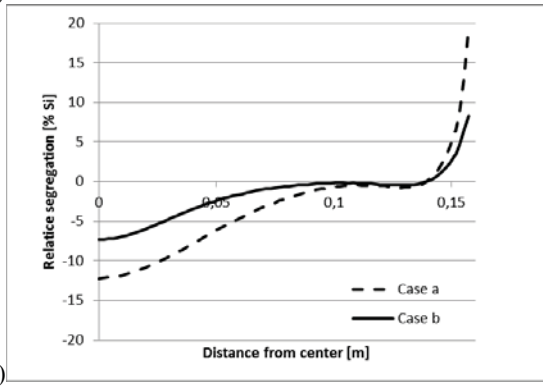

(b)

Figure 6: Si segregation. a) Segregation pattern (wt %) for case a and b (white line at fs=1). b) Segregation (%) in the steady state from center to surface of the ingot.

The computed Cu segregation pattern is shown in Figure 7a, whereas the concentration profile from the center to the surface of the ingot is shown if Figure 7b. The segregation pattern of case a) and b) differ only slightly. Along the surfaces of the ingot ~20% and ~18% positive relative segregation is obtained for case a) and b) respectively. In the center of the ingot, ~12% and 10% negative segregation is obtained for case a) and b) respectively. The precipitation of Cu containing particles starts at a solid fraction of approximately 0.98 (Figure 2) with a minor effect on the distribution of Cu between the liquid and solid phase during solidification.

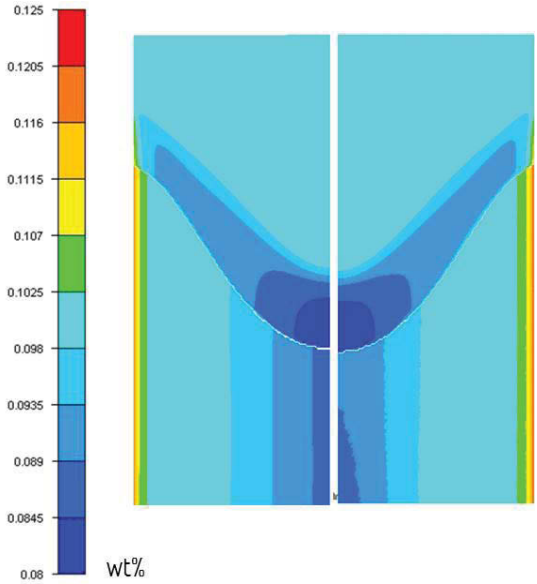

(a)

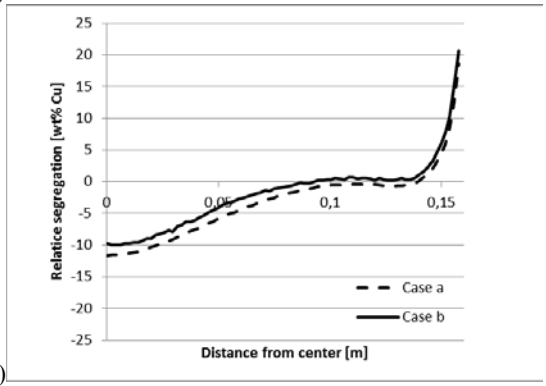

(b)

Figure 7: Cu segregation. a) Segregation pattern (wt %) for case a and b (white line at fs=1). b) Segregation (%) in the steady state from center to surface of the ingot.

Summary

The continuum model Alsim has been coupled with the microsegregation model Alstruc in order to compute macrosegregation for multicomponent Al alloys. The module has been used in a case study on DC-casting to illustrate the effect of secondary phase precipitation on macrosegregation formation due to shrinkage induced flow. Significant differences are observed demonstrating the usefulness of the proposed coupling approach using the Alstruc module, and emphasizing the need for an accurate description of the distribution of solute elements between the liquid and solid phase in the calculation of macrosegregation.

Acknowledgements

Funding of this work by the MINAC-project (Modelling assisted Innovation for the Aluminium DC Casting process) is gratefully acknowledged. Partners in MINAC were Alcoa Norway ANS, Aleris Rolled Products Germany GmbH, Hydro Aluminium ASA, Materials innovation institute (M2i), Stiftelsen SINTEF and Institute for Energy Technology (IFE). The project was supported by the Norwegian research council through the BIA programme.

References

1. A.L. Dons, E.K. Jensen, Y. Langsrud, E. Trømborg and S. Brusethaug: Metallurgical and Materials Transactions A, 1999, 30A, 2135–2146.
2. D. Mortensen: Metallurgical and Materials Transactions B, 1999, 30B, 119–133.
3. H. Combeau, J.M. Drezet, A. Mo and M. Rappaz: Metallurgical and Materials Transactions A, 1996, 27A, 2314–2327.
4. H. Feufel, T. Godecke, H.L. Lukas and F. Sommer: Journal of Alloys and compounds, 1997, 247, 31–42.
5. N. Saunders: in 'Light Metals' (ed. R. Huglen), TMS, Warrendale, PA, 1997, 911–918.
6. N. Saunders: Al-DATA, a thermodynamic database for calculation of phase equilibria in multicomponent Al-based alloys V. 2.0, Technical report, Thermotech Ltd, Surrey Technology Centre, The Surrey Research park, UK, 1998.
7. I. Ansara, A.T. Dinsdale and M.H. Randet (editors): COST 507, Thermochemical database for light metal alloys, Vol.2, Technical Report ISBN 92-828-3902-8, Office for Official Publications of the European Communities, Luxembourg, 1998.
8. D.K. Banerjee, M.T. Samonds, U.R. Kattner and W.J. Boettinger: Proc. Int. Conf. Solidification Processing IV (eds. J. Beech and H. Jones), University of Sheffield, 1997, 354–357.
9. X. Doré, H. Combeau and M. Rappaz: Acta Materialia, 2000, 48, 3951–3962.
10. S.A. Cefalu and M. J. M. Krane: Material Science and Engineering A, 2003, 359, 91–99.
11. Q. Du and A. Jacot: Acta Materiala, 2005, 53, 3479–3493.
12. Q. Du, D.G. Eskin and L. Katgerman: Metallurgical and Materials Transactions A, 2007, 38A, 180–198.
13. A. Mo and H. J. Thevik: Metallurgical and Materials Transactions A, 1999, 29A, 2189-94
14. K. Ellingsen, Q. Du, A. Mo and M. M'Hamdi: Proc. Int. Conf. Solidification Processing V (ed. H. Jones), The University of Sheffield, 2007, 442–446.
15. K.Ellingsen, A. L. Dons, M. M'Hamdi, A. Mo, and D. Mortensen: Int. J. Cast Met. Res., 2009, 22, NO 1-4.
16. H.G. Fjær and A. Mo: Metallurgical Transactions B, 1990, 21B, 1049–1061.
17. H.J. Thevik, A. Mo and T. Rusten: Metallurgical and Materials Transactions B, 1999, 30B, 135–142.
18. D. Mortensen, B.R. Henriksen, M. M'Hamdi and H.G. Fjær: in 'Light Metals' (ed. D. H. DeYoung), TMS, Warrendale, PA, 2008, 773–779.
19. M. M'Hamdi, A. Mo and H.G. Fjær: Metallurgical and Materials Transactions A, 2006, 37A, 3069–3083.
20. A.L. Dons: Zeitschrift für Metallkunde, 1990, 81, 484–489.
21. A.L. Dons: Zeitschrift für Metallkunde, 1991, 82, 684–688.
22. A.L. Dons, E.K. Jensen, J. Voje and J. Rødseth: Proc. Int. Conf. Modelling of Casting, Welding and Advanced Solidification Processes VI (eds. T. S. Piwonka, Voller and Katgerman.), TMS, Warrendale, PA, 1993, 37–44.
23. A.L. Dons, S. Brusethaug and J. Voje: Proc. Int. Conf. Modelling of casting, welding and advanced solidification processes – VIII (eds. C. Beckermann and B. G. Thomas), TMS, Warrendale, PA, 1998, 195–202.
24. A.L. Dons, L. Pedersen and L. Arnberg: Materials Science and Engineering, 1999, A271, 91–94.
25. J. Voje and A.L. Dons: Aluminium, 2001, 77, 284–287.
26. K. Ellingsen, A. L. Dons, M. M'Hamdi, D. Mortensen, International Conference on Modeling of Casting, Welding, and Advanced Solidification Processes, 12, Vancouver, Canada, 2009-06-07--06-14. Proceedings, 651-657.
27.] Weckman, D.C. and P. Niessen, Metallurgical Transactions B, 1982. 13(4): p. 593-602.